Texture Analysis of Dorsal Striatum in Functional Neurological (Conversion) Disorder

Murat Baykara (muratbaykara@hotmail.com)
Firat Universitesi Tip Fakultesi https://orcid.org/0000-0003-2588-9013
Sema Baykara
Firat Universitesi Tip Fakultesi

Research Article

Keywords: Conversion disorder, caudate nucleus, putamen, image processing, computer-assisted, magnetic resonance imaging

Posted Date: June 8th, 2021

DOI: https://doi.org/10.21203/rs.3.rs-501944/v1

Abstract

In this study, it was aimed to evaluate the dorsal striatum nuclei of patients diagnosed with Functional Neurological Disorder by tissue analysis method from magnetic resonance imaging images and to compare them with healthy controls.

Study groups consisted of 20 female patients and 20 healthy women. The brains of patients and controls were scanned for high-resolution images with a 1.5 T scanner using the sagittal plane and 3D spiral fast spin echo sequence. Using the texture analysis method, mean, standard deviation, minimum, maximum, median, variance, entropy, size %L, size %U, size %M, kurtosis, skewness and homogeneity values of the dorsal striatum nuclei were calculated from the images. The data were compared with comparison tests according to Kolmogorov-Smirnov test results.

There was no statistically significant difference between paired regions in terms of texture analysis findings in the cross-sectional images of the participants. In patients, mean, standard deviation, minimum, maximum, median, variance and entropy values for the putamen nucleus, and mean, standard deviation, minimum, maximum, median, variance, entropy and kurtosis values for the caudate nucleus were found significantly higher than controls. Additional receiver operating characteristic curve and logistic regression analyzes were performed.

The implications of the results of the study are that there are significant microstructural changes in the dorsal striatum nuclei of patients and their reflection on brain images. Texture analysis is a useful technique to show tissue changes in the dorsal striatum of patients using images. It is highly recommended to use tissue analysis to identify and evaluate potentially affected areas of the brain in new studies.

Introduction

Functional Neurological Disorder (FND) is a condition that cannot be defined and clarified by neurological symptoms and medical conditions that can develop typical neurological diseases (Aybek et al., 2015). Its etiology has not been clearly elucidated, but the number and emphasis of neurobiological explanations has increased in recent years (Atmaca, Baykara, Mermi, Yildirim, & Akaslan, 2016; Aybek, Nicholson, Draganski, et al., 2014; S. Baykara, Baykara, Mermi, Yildirim, & Atmaca, 2021; Vuilleumier, 2014). Psychogenic trauma is a risk factor for FND, and clinical findings suggest that altered emotional processing and motor symptoms are closely linked to it. However, it is not clearly understood which neural networks interact in this process (Aybek, Nicholson, Zelaya, et al., 2014). Recent studies have revealed the presence of impressive brain findings in FND that can be recognized by imaging (Atmaca et al., 2016; Aybek et al., 2015; S. Baykara et al., 2021; Giedd, Raznahan, Mills, & Lenroot, 2012).

As is known, a two-dimensional digital image used in routine clinical practice consists of small rectangular blocks (image elements) called pixels (Castellano, Bonilha, Li, & Cendes, 2004). Pixels represent points in the spatial coordinates of the image and each has a value representing the gray level intensity at that point in the image (Castellano et al., 2004). Various mathematical methods are used to determine the spatial gray level variations in the image, which are constituent derivatives called "texture properties" and provide a measure of heterogeneity and called texture analysis (Sema Baykara, Baykara, Mermİ, Yildirim, & Atmaca, 2021). The position and intensity features of the pixels in the images are analyzed by texture analysis techniques (Murat Baykara, Koca, Demirel, Berk, & and, 2018).

These techniques, including histogram analysis based on statistics, are increasingly used in many studies that investigate structural differences (Murat Baykara et al., 2018; Castellano et al., 2004), diagnose diseases (Murat Baykara et al., 2018; Castellano et al., 2004), identifying diagnostic and prognostic biomarkers (Alic, Niessen, & Veenland, 2014; Molina et al., 2016a; Yang, Rao, Martinez, Veeraraghavan, & Rao, 2015), characterize tumors (Tixier et al., 2012; Yang et al., 2015), and guiding treatment (Molina et al., 2016b; Yang et al., 2015).

The role of the striatum in the regulation and control of motor movement has long been recognized. Recently, frontal corticobasal ganglia networks have been described and attention has been drawn to the role of the dorsal striatum in executive functions. New discoveries show that the dorsal striatum directly contributes, in particular, action selection and initiation, decision-making, through the integration of sensory-motor, cognitive, and motivational / emotional information in specific corticostriatal circuits, including the striatum (Atmaca, Aydin, Tezcan, Poyraz, & Kara, 2006; Balleine, Delgado, & Hikosaka, 2007; Vuilleumier, 2014; Vuilleumier et al., 2001).

Because of the important findings in recent studies, we aimed to evaluate the striatum by tissue (histogram) analysis using T1-weighted magnetic resonance imaging (MRI) images of patients with FND and to compare the findings with healthy controls.

Methods

Local Ethics Committee approval was obtained (date: 03/28/2013, session: 05, decision: 02). The criteria of the study were determined as being between 18 and 65 years of age, having no other psychiatric diagnosis, no mental retardation, no neurological or physiological disease, no history of alcohol or substance use in the last 6 months, and no contraindications for MRI examinations.

Study population

Twenty female patients who applied to the psychiatry outpatient clinic and were diagnosed with FND according to the Diagnostic and Statistical Manual of Mental Disorders-5 (DSM-5) (American Psychiatric Association. & American Psychiatric Association. DSM-5 Task Force., 2013) criteria and whose first symptom was psychogenic non-epileptic seizures (PNES) were studied. The diagnosis of the patients was confirmed after a psychiatric evaluation by a psychiatrist with 15 years of experience. Patients had been using selective serotonin reuptake inhibitors or tricyclic antidepressants for at least the past four months, whose doses were stabilized two months prior to the study.

The criteria of the study were determined as based on information obtained hospital information system and using patient statements, being between 18–65 years of age, having no other psychiatric diagnosis, no mental retardation, no neurological or physiological disease, no history of alcohol or substance use in the last 6 months and no contraindications for MRI examination.

Twenty healthy individuals who met the above-mentioned study criteria, having no psychiatric diagnosis and equivalent in terms of age and gender were determined as the control group. All participants signed an informed consent form and then had an MRI examination.

Imaging process

1.5T General Electric Signa Excite scanner (GE, Milwaukee, Wisconsin, USA) was used for MRI. Spiral pulse sequences were used due to insensitivity to subject movement. A high resolution structural image of the entire brain was obtained using 3D spiral fast spin echo high resolution images obtained sagittally (TR = 2000 ms, TE = 15.6 ms, TI = 700 ms, FOV = 240 mm, echo spacing = 15.6 ms, 8 echoes, resolution = 0.9375×0.9375×1.328 mm, 128 contiguous slices, 8 min 36 s). Axial and coronal images were reformatted from sagittal acquisitions.

Analysis of images

MRI images were transferred in DICOM 3.0 format to a 27-inch iMac computer (Apple Inc., Cupertino, CA, USA) and processed with OsiriX V.4.9 imaging software (Pixmeo, Switzerland). In OsiriX software, a region of interest (ROI) was placed on each of the bilateral putamen and caudate nuclei in the axial plane images, without exceeding their boundaries in the section where they are the largest (Fig. 1). The values of the pixels inside each ROI were saved in XML (eXtensible Markum Language) format and transferred to a computer running MATLAB software (version R2017a; MathWorks, Natick, MA, USA) on Windows 10 operating system (Microsoft Corporation, One Microsoft Way Redmond, WA 98052, USA). The whole texture analysis algorithm was implemented with an in-house software coded in MATLAB from ROI values taken from XML files.

The mean, standard deviation, median, minimum, maximum, variance, entropy, uniformity, skewness, kurtosis, size %L, size %M and size %U values obtained from the gray level intensities of the pixels in the ROIs have been previously described in the literature (Sema Baykara et al., 2021; Castellano et al., 2004).

Statistical analysis

Statistical analyzes were performed with IBM SPSS for Windows, version 25.0 (IBM statistics for Windows version 25, IBM Corporation, Armonk, New York, USA). Data are presented as mean ± standard deviation. The normality of the distribution was evaluated by Kolmogorov-Smirnov test, and Student t test, Mann-Whitney U test, one-way ANOVA test and Kruskal-Wallis test were used to compare the groups according to the results of this test. A p value of < 0.05 was considered statistically significant.

Results

All patients and control individuals were female, the mean age of the patient group was 33.71 ± 9.93, the mean age of the control group was 32.75 ± 8.50, and there was no significant difference in age between the groups ($p = 0.744$).

As seen in Table 1, there was no statistically significant difference between paired regions in the cross-sectional images of neither patients nor control individuals ($p > 0.05$).

The mean, standard deviation, minimum, maximum, median, variance and entropy values for the putamen nucleus, and mean, standard deviation, minimum, maximum, median, variance, entropy and kurtosis values for the caudate nucleus in patients with FND were found statistically significantly higher than controls (Table 2 and Fig. 2). There was no significant difference in FND patients compared to control individuals in terms of other parameters.

When ROC analyzes (Fig. 3) are performed for statistically significant values, the calculated AUC values, and the sensitivity and specificity values when a threshold value is chosen to distinguish the two groups from each other are shown in Table 3.

Logistic regressions were performed for each two nuclei values to determine the effects of mean, standard deviation, minimum, maximum, median, variance, entropy and kurtosis (only for caudate) on the likelihood that participants have FND (Table 4). The logistic regression models were statistically significant, $\chi^2(7) = 17.438$, $p < 0.001$ for putamen and $\chi^2(8) = 24.872$, $p < 0.001$ for caudate. This models explained 91.9% (Nagelkerke R^2) of the variance in FND for putamen and 87.8% for caudate nuclei, and correctly classified 97.5% of cases for putamen and 93.8% for caudate nuclei. Increasing mean and standard deviation were associated with an increased likelihood of exhibiting FND, but increasing maximum, median and entropy were associated with a reduction in the likelihood of exhibiting FND for putamen (Table 4). Also, increasing standard deviation was associated with an increased likelihood of exhibiting FND, but increasing entropy was associated with a reduction in the likelihood of exhibiting FND for caudate.

Discussion

The absence of abnormal findings in imaging results since the 19th century has been thought to be a supporting factor for the clinician in the diagnosis of FND (Atmaca et al., 2016). However, the perspective on FND has changed, mainly with studies evaluating the neurobiology of FND based on functional neuroimaging studies (Aybek, Nicholson, Draganski, et al., 2014; Aybek et al., 2015; Aybek, Nicholson, Zelaya, et al., 2014; Reynolds, 2012).

Increasing evidence has recently proven that texture analysis is an important computer-aided diagnostic method (Kurtul & Baykara, 2018; McLaren, Chen, Nie, & Su, 2009; Yang et al., 2015). Texture analysis is a post-processing technique that includes descriptive statistics that allow measurement of a range of pixel dispersion parameters such as entropy, uniformity, kurtosis, skewness, average gray level intensity and standard deviation (M. Baykara & Sagiroglu, 2019; S. Baykara et al., 2021; Yildirim & Baykara, 2020). This analysis identifies structures that cannot be assessed visually based on an explanation of microstructural

information and provides more valuable information about structural models than shape-based measurements (Aybek, Nicholson, Draganski, et al., 2014; Latha & Kavitha, 2018; Radulescu et al., 2014). Recently, the evaluation of brain MRI images with texture analysis methods has become the focus of attention in the investigation of the etiology of psychiatric disorders (Latha & Kavitha, 2018; Radulescu et al., 2014).

Evaluations by texture analysis of brain MRI images provide a high-powered tool for assessing differences in complexity in cortical and subcortical gray matter. It also allows the measurement of the gray level pattern in images through pixel relationships and dispersion properties. This means it is a more accessible and engaging research tool for neurology and psychiatry (Kassner & Thornhill, 2010; Radulescu et al., 2014).

Studies show that potential advances in tissue analysis are beneficial when applied to neuropsychiatric disorders such as attention deficit hyperactivity disorder [31], multiple sclerosis [30], Parkinson's disease (Hett et al., 2021), functional neurological disorder [9], epilepsy [28, 29], and Alzheimer's disease (Sudheesh & Basavaraj, 2021).

A study examining brain MRI images with tissue analysis showed that the entropy and homogeneity of gray matter in schizophrenia differed significantly from healthy controls, emphasizing the abnormal distribution of gray matter and changes in the focal structure of the hippocampus (Radulescu et al., 2014).

In the literature review, it was seen that the dorsal striatum was not analyzed by texture analysis in patients with FND before. In present study, a statistical approach has been adopted that determines the texture information in images based on the gray level distribution of pixels in medical imaging, giving better results than older methods such as structural approaches (Alam & Faruqui, 2011; Dhruv, Mittal, & Modi, 2019; Haralick, 1979; Yildirim & Baykara, 2020).

Although there was no visual difference between the dorsal striatum nucleus regions in axial MRI images of FND patients and controls in present study; mean, standard deviation, maximum, median, variance, entropy and size %M values were higher, and size %U values were lower in the putamen nuclei of the patients with FND. In addition, mean, standard deviation, minimum, maximum, median, variance, entropy and kurtosis values were significantly higher in the caudate nuclei of the patients with FND compared to the control group.

According to the literature, the findings of present study show that the gray level distribution in the dorsal striatum nuclei becomes irregular and inhomogeneity in intensity increases in patients with FND compared to the control group (Murat Baykara et al., 2018; S. Baykara et al., 2021; Ganeshan, Miles, Young, & Chatwin, 2007, 2009; Suo et al., 2016).

ROC and regression analyses performed in present study show that FND patients can be distinguished from healthy individuals by using texture information in brain MRI images.

Limitations

This present study has some limitations. Since there were no previous studies evaluating dorsal striatum nuclei with tissue analysis in patients with FND, the study findings could not be compared. In addition, the fact that all FND patients and therefore the selected controls were women prevented the study findings from being generalized to both genders.

Conclusion

The implications of the results of this study are that there are significant microstructural changes in the dorsal striatum nuclei of patients with FND, and these are reflected in brain MRI images, even if they are not visible to the naked eye. However, whether this is a cause or effect is beyond the scope of this study, and further studies are needed that could further contribute to determining the etiology of FND and its diagnosis and treatment options. Texture analysis is a useful technique to show tissue changes in the dorsal striatum of patients with FND using MRI images. It is highly recommended to use texture analysis to identify and evaluate potentially affected areas of the brain in new studies.

Declarations

Acknowledgments

Author Contributions

Author contributions included conception and study design (MB and SB), data collection or acquisition (SB), statistical analysis (MB), interpretation of results (MB and SB), drafting the manuscript work or revising it critically for important intellectual content (MB and SB) and approval of final version to be published and agreement to be accountable for the integrity and accuracy of all aspects of the work (MB and SB).

Funding Sources

This research was financially supported by Firat University Scientific Research Projects Unit (FUBAP Project No: TF.13.40).

Compliance with Ethical Standards

The local Firat University Non-Interventional Researchs Ethics Committee have reviewed and approved the study protocol described in the manuscript.

Conflict of Interest

None of the authors have a conflict of interest to declare.

References

Alam, F. I., & Faruqui, R. U. (2011). Optimized calculations of haralick texture features. *European Journal of Scientific Research, 50*(4), 543-553.

Alic, L., Niessen, W. J., & Veenland, J. F. (2014). Quantification of heterogeneity as a biomarker in tumor imaging: a systematic review. *PLoS One, 9*(10), e110300. doi:10.1371/journal.pone.0110300

American Psychiatric Association., & American Psychiatric Association. DSM-5 Task Force. (2013). *Diagnostic and statistical manual of mental disorders : DSM-5* (5th ed.). Washington, D.C.: American Psychiatric Association.

Atmaca, M., Aydin, A., Tezcan, E., Poyraz, A. K., & Kara, B. (2006). Volumetric investigation of brain regions in patients with conversion disorder. *Prog Neuropsychopharmacol Biol Psychiatry, 30*(4), 708-713. doi:10.1016/j.pnpbp.2006.01.011

Atmaca, M., Baykara, S., Mermi, O., Yildirim, H., & Akaslan, U. (2016). Pituitary volumes are changed in patients with conversion disorder. *Brain Imaging Behav, 10*(1), 92-95. doi:10.1007/s11682-015-9368-6

Aybek, S., Nicholson, T. R., Draganski, B., Daly, E., Murphy, D. G., David, A. S., & Kanaan, R. A. (2014). Grey matter changes in motor conversion disorder. *J Neurol Neurosurg Psychiatry, 85*(2), 236-238. doi:10.1136/jnnp-2012-304158

Aybek, S., Nicholson, T. R., O'Daly, O., Zelaya, F., Kanaan, R. A., & David, A. S. (2015). Emotion-motion interactions in conversion disorder: an FMRI study. *PLoS One, 10*(4), e0123273. doi:10.1371/journal.pone.0123273

Aybek, S., Nicholson, T. R., Zelaya, F., O'Daly, O. G., Craig, T. J., David, A. S., & Kanaan, R. A. (2014). Neural correlates of recall of life events in conversion disorder. *JAMA Psychiatry, 71*(1), 52-60. doi:10.1001/jamapsychiatry.2013.2842

Balleine, B. W., Delgado, M. R., & Hikosaka, O. (2007). The role of the dorsal striatum in reward and decision-making. *J Neurosci, 27*(31), 8161-8165. doi:10.1523/JNEUROSCI.1554-07.2007

Baykara, M., Koca, T. T., Demirel, A., Berk, E., & and, a. (2018). Magnetic resonance imaging evaluation of the median nerve using histogram analysis in carpal tunnel syndrome. *Neurological Sciences and Neurophysiology*, 145-150.

Baykara, M., & Sagiroglu, S. (2019). An evaluation of magnetic resonance imaging with histogram analysis in patients with idiopathic subjective tinnitus. *North Clin Istanb, 6*(1), 59-63. doi:10.14744/nci.2018.72593

Baykara, S., Baykara, M., Mermi, O., Yildirim, H., & Atmaca, M. (2021). Magnetic resonance imaging histogram analysis of corpus callosum in a functional neurological disorder. *Turk J Med Sci, 51*(1), 140-147. doi:10.3906/sag-2004-252

Baykara, S., Baykara, M., Mermİ, O., Yildirim, H., & Atmaca, M. (2021). Magnetic resonance imaging histogram analysis of corpus callosum in a functional neurological disorder. *Turkish journal of medical sciences, 51*(1), 140-147.

Castellano, G., Bonilha, L., Li, L. M., & Cendes, F. (2004). Texture analysis of medical images. *Clin Radiol, 59*(12), 1061-1069. doi:10.1016/j.crad.2004.07.008

Dhruv, B., Mittal, N., & Modi, M. (2019). Study of Haralick's and GLCM texture analysis on 3D medical images. *Int J Neurosci, 129*(4), 350-362. doi:10.1080/00207454.2018.1536052

Ganeshan, B., Miles, K. A., Young, R. C., & Chatwin, C. R. (2007). Hepatic entropy and uniformity: additional parameters that can potentially increase the effectiveness of contrast enhancement during abdominal CT. *Clin Radiol, 62*(8), 761-768. doi:10.1016/j.crad.2007.03.004

Ganeshan, B., Miles, K. A., Young, R. C., & Chatwin, C. R. (2009). Texture analysis in non-contrast enhanced CT: impact of malignancy on texture in apparently disease-free areas of the liver. *Eur J Radiol, 70*(1), 101-110. doi:10.1016/j.ejrad.2007.12.005

Giedd, J. N., Raznahan, A., Mills, K. L., & Lenroot, R. K. (2012). Review: magnetic resonance imaging of male/female differences in human adolescent brain anatomy. *Biol Sex Differ, 3*(1), 19. doi:10.1186/2042-6410-3-19

Haralick, R. M. (1979). Statistical and structural approaches to texture. *Proceedings of the IEEE, 67*(5), 786-804.

Hett, K., Lyu, I., Trujillo, P., Lopez, A. M., Aumann, M., Larson, K. E., . . . Claassen, D. O. (2021). Anatomical texture patterns identify cerebellar distinctions between essential tremor and Parkinson's disease. *Human Brain Mapping*.

Kassner, A., & Thornhill, R. E. (2010). Texture analysis: a review of neurologic MR imaging applications. *AJNR Am J Neuroradiol, 31*(5), 809-816. doi:10.3174/ajnr.A2061

Kurtul, N., & Baykara, M. (2018). The association between MRI texture analysis and chemoradiotherapy outcomes in glioblastoma cases. *Ann Med Res, 25*(4), 1.

Latha, M., & Kavitha, G. (2018). Segmentation and texture analysis of structural biomarkers using neighborhood-clustering-based level set in MRI of the schizophrenic brain. *MAGMA, 31*(4), 483-499. doi:10.1007/s10334-018-0674-z

McLaren, C. E., Chen, W. P., Nie, K., & Su, M. Y. (2009). Prediction of malignant breast lesions from MRI features: a comparison of artificial neural network and logistic regression techniques. *Acad Radiol, 16*(7), 842-851. doi:10.1016/j.acra.2009.01.029

Molina, D., Perez-Beteta, J., Luque, B., Arregui, E., Calvo, M., Borras, J. M., . . . Perez-Garcia, V. M. (2016a). Tumour heterogeneity in glioblastoma assessed by MRI texture analysis: a potential marker of survival. *Br J Radiol, 89*(1064), 20160242. doi:10.1259/bjr.20160242

Molina, D., Perez-Beteta, J., Luque, B., Arregui, E., Calvo, M., Borras, J. M., . . . Perez-Garcia, V. M. (2016b). Tumour heterogeneity in glioblastoma assessed by MRI texture analysis: a potential marker of survival. *Br J Radiol*, 20160242. doi:10.1259/bjr.20160242

Radulescu, E., Ganeshan, B., Shergill, S. S., Medford, N., Chatwin, C., Young, R. C., & Critchley, H. D. (2014). Grey-matter texture abnormalities and reduced hippocampal volume are distinguishing features of schizophrenia. *Psychiatry Res, 223*(3), 179-186. doi:10.1016/j.pscychresns.2014.05.014

Reynolds, E. H. (2012). Hysteria, conversion and functional disorders: a neurological contribution to classification issues. *Br J Psychiatry, 201*(4), 253-254. doi:10.1192/bjp.bp.111.107219

Sudheesh, K., & Basavaraj, L. (2021). Qualitative Approach of Empirical Mode Decomposition-Based Texture Analysis for Assessing and Classifying the Severity of Alzheimer's Disease in Brain MRI Images. In *Advances in Artificial Intelligence and Data Engineering* (pp. 1227-1253): Springer.

Suo, S. T., Zhuang, Z. G., Cao, M. Q., Qian, L. J., Wang, X., Gao, R. L., . . . Xu, J. R. (2016). Differentiation of pyogenic hepatic abscesses from malignant mimickers using multislice-based texture acquired from contrast-enhanced computed tomography. *Hepatobiliary Pancreat Dis Int, 15*(4), 391-398.

Tixier, F., Hatt, M., Le Rest, C. C., Le Pogam, A., Corcos, L., & Visvikis, D. (2012). Reproducibility of tumor uptake heterogeneity characterization through textural feature analysis in 18F-FDG PET. *J Nucl Med, 53*(5), 693-700. doi:10.2967/jnumed.111.099127

Vuilleumier, P. (2014). Brain circuits implicated in psychogenic paralysis in conversion disorders and hypnosis. *Neurophysiol Clin, 44*(4), 323-337. doi:10.1016/j.neucli.2014.01.003

Vuilleumier, P., Chicherio, C., Assal, F., Schwartz, S., Slosman, D., & Landis, T. (2001). Functional neuroanatomical correlates of hysterical sensorimotor loss. *Brain, 124*(Pt 6), 1077-1090.

Yang, D., Rao, G., Martinez, J., Veeraraghavan, A., & Rao, A. (2015). Evaluation of tumor-derived MRI-texture features for discrimination of molecular subtypes and prediction of 12-month survival status in glioblastoma. *Med Phys, 42*(11), 6725-6735. doi:10.1118/1.4934373

Yildirim, M., & Baykara, M. (2020). Differentiation of Multiple Myeloma and Lytic Bone Metastases: Histogram Analysis. *J Comput Assist Tomogr, 44*(6), 953-955. doi:10.1097/RCT.0000000000001086

Tables

Table 1. Distribution of values of analyzed parameters of putamen and caudate nuclei of the groups.

	Putamen										Caudate		
	Functional Neurological Disorder (40)					Control (40)					Functional Neurological I		
	Right (20)		Left (20)		p	Right (20)		Left (20)		p	Right (20)		Left
	Mean	S.D.	Mean	S.D.		Mean	S.D.	Mean	S.D.		Mean	S.D.	Mea
Mean	***440.56***	***45.90***	***434.64***	***45.64***	***0.678*****	***320.51***	***137.61***	***309.48***	***131.25***	***0.678*****	***<0.001****	***428.87***	***43.02***	***426***
Standard Deviation	***15.46***	***3.38***	***15.90***	***3.47***	***0.689††***	***11.25***	***4.53***	***13.53***	***6.20***	***0.192††***	***0.007†***	***20.09***	***4.79***	***19.2***
Minimum	***399.90***	***47.85***	***390.45***	***44.31***	***0.398*****	***291.35***	***128.75***	***276.25***	***119.44***	***0.547*****	***<0.001****	***367.45***	***55.06***	***370***
Maximum	***479.40***	***47.68***	***474.90***	***49.99***	***0.758*****	***346.25***	***147.10***	***342.25***	***145.13***	***0.904*****	***<0.001****	***477.75***	***47.98***	***478***
Median	***441.28***	***45.72***	***435.13***	***45.81***	***0.640*****	***320.68***	***137.76***	***310.20***	***131.46***	***0.678*****	***<0.001****	***428.95***	***43.43***	***426***
Variance	***249.89***	***106.42***	***264.16***	***119.51***	***0.692††***	***146.00***	***113.09***	***219.54***	***180.01***	***0.130††***	***0.030†***	***425.55***	***230.95***	***389***
Entropy	***5.66***	***0.28***	***5.68***	***0.26***	***0.947*****	***5.03***	***0.46***	***5.18***	***0.52***	***0.398*****	***<0.001****	***5.85***	***0.24***	***5.88***
Size %L	15.81	2.06	16.27	2.06	0.486††	15.16	2.03	16.00	2.24	0.222††	0.390†	14.66	3.67	15.4
Size %U	15.81	2.82	15.73	2.33	0.920††	14.88	1.93	14.87	2.30	0.983††	0.412†	16.06	2.45	15.5
Size %M	68.37	4.34	68.00	3.67	0.769††	69.96	2.70	69.14	3.67	0.423††	0.337†	69.27	4.69	69.0
Kurtosis	3.02	0.74	2.99	0.65	0.820**	3.02	0.51	3.10	1.08	0.314**	0.815*	***3.64***	***1.62***	***3.51***
Skewness	-0.13	0.42	-0.16	0.25	0.792††	-0.17	0.40	-0.17	0.53	0.969††	0.986†	-0.22	0.57	-0.06
Uniformity	0.30	0.07	0.31	0.05	0.512††	0.33	0.06	0.31	0.08	0.465††	0.578†	0.34	0.10	0.30

S.D.: Standard Deviation, *Kruskal-Wallis Test, **Mann-Whitney U Test, †One-Way ANOVA with Tukey HSD, ††Independent-Samples T Test

Table 2. Distribution of values of analyzed parameters of putamen and caudate nuclei of the groups.

	Putamen					Caudate				
	Functional Neurological Disorder (40)		Control (40)		p	Functional Neurological Disorder (40)		Control (40)		p
	Mean	S.D.	Mean	S.D.		Mean	S.D.	Mean	S.D.	
Mean	***437.60***	***45.28***	***314.99***	***132.85***	***<0.001****	***427.55***	***42.41***	***305.37***	***130.78***	***<0.001****
Standard Deviation	***15.68***	***3.39***	***12.39***	***5.49***	***0.002†***	***19.68***	***4.54***	***12.98***	***6.51***	***<0.001†***
Minimum	***395.18***	***45.77***	***283.80***	***122.81***	***<0.001****	***369.20***	***51.68***	***270.48***	***117.76***	***<0.001****
Maximum	***477.15***	***48.27***	***344.25***	***144.25***	***<0.001****	***478.15***	***48.66***	***333.50***	***142.49***	***<0.001****
Median	***438.20***	***45.28***	***315.44***	***133.01***	***<0.001****	***427.48***	***42.51***	***305.68***	***131.01***	***<0.001****
Variance	***257.02***	***111.93***	***182.77***	***152.98***	***0.015****	***407.31***	***202.32***	***209.85***	***204.73***	***<0.001****
Entropy	***5.67***	***0.26***	***5.11***	***0.49***	***<0.001****	***5.86***	***0.25***	***5.00***	***0.50***	***<0.001****
Size %L	16.04	2.05	15.58	2.15	0.325†	15.04	3.12	16.22	3.39	0.109†
Size %U	15.77	2.56	14.87	2.09	0.089†	15.81	2.40	15.92	2.92	0.851†
Size %M	68.19	3.97	69.55	3.21	0.095†	69.15	4.23	67.85	5.30	0.231†
Kurtosis	3.01	0.68	3.06	0.84	0.900*	***3.57***	***1.60***	***3.21***	***1.57***	***0.044****
Skewness	-0.14	0.34	-0.17	0.47	0.760†	-0.14	0.52	-0.20	0.49	0.564†
Uniformity	0.31	0.06	0.32	0.07	0.320†	0.32	0.10	0.35	0.09	0.180†

S.D.: Standard Deviation, *Mann-Whitney U Test, †Independent-Samples T Test

Table 3. ROC analysis values of analyzed parameters of putamen and caudate nuclei of the groups.

	Putamen				Caudate			
	Area under the curve (AUC)	Threshold	Sensitivity (%)	Specificity (%)	Area under the curve (AUC)	Threshold	Sensitivity (%)	Specificity (%)
Mean	0.802	390.948	87.5	72.5	0.802	392.954	75.0	75.0
Standard deviation	0.691	14.08	65.0	67.5	0.794	16.457	82.5	75.0
Minimum	0.810	367.50	75.0	77.5	0.779	347.50	77.5	77.5
Maximum	0.794	445	77.5	77.5	0.799	434	85.0	77.5
Median	0.803	406	77.5	72.5	0.803	392.5	72.5	72.5
Variance	0.691	192.313	67.5	65.0	0.794	289.648	75.0	75.0
Entropy	0.820	5.5	67.5	67.5	0.942	5.59	90.0	87.5
Kurtosis					0.631	2.843	60.0	60.0

Table 4. Logistic regression analysis values of statistically significant parameters of analyzed putamen and caudate nuclei of the groups.

	Putamen								Caudate						
	B	S.E.	Wald	df	Sig.	Exp(B)	95% C.I. for EXP(B)		B	S.E.	Wald	df	Sig.	Exp(B)	95% C.I. EXP(B)
							Lower	Upper							Lower
Mean	***2.762***	***1.268***	***4.744***	***1***	***0.029***	***15.825***	***1.318***	***189.936***	-0.165	0.455	0.132	1	0.716	0.847	0.347
Standard Deviation	***6.586***	***2.845***	***5.358***	***1***	***0.021***	***724.729***	***2.744***	***191440.282***	***1.595***	***0.784***	***4.138***	***1***	***0.042***	***4.931***	***1.06***
Minimum	0.105	0.104	1.025	1	0.311	1.111	0.906	1.362	-0.038	0.084	0.21	1	0.647	0.962	0.817
Maximum	***-0.256***	***0.122***	***4.413***	***1***	***0.036***	***0.774***	***0.61***	***0.983***	-0.074	0.11	0.453	1	0.501	0.928	0.748
Median	***-2.651***	***1.248***	***4.515***	***1***	***0.034***	***0.071***	***0.006***	***0.814***	0.27	0.395	0.467	1	0.494	1.31	0.604
Variance	-0.084	0.066	1.632	1	0.201	0.919	0.808	1.046	-0.018	0.02	0.758	1	0.384	0.983	0.944
Entropy	***-37.369***	***12.652***	***8.723***	***1***	***0.003***	***0.000***	***0.000***	***0.000***	***-16.999***	***5.965***	***8.12***	***1***	***0.004***	***0.000***	***0.000***
Kurtosis									-1.168	0.898	1.691	1	0.194	0.311	0.054

Figures

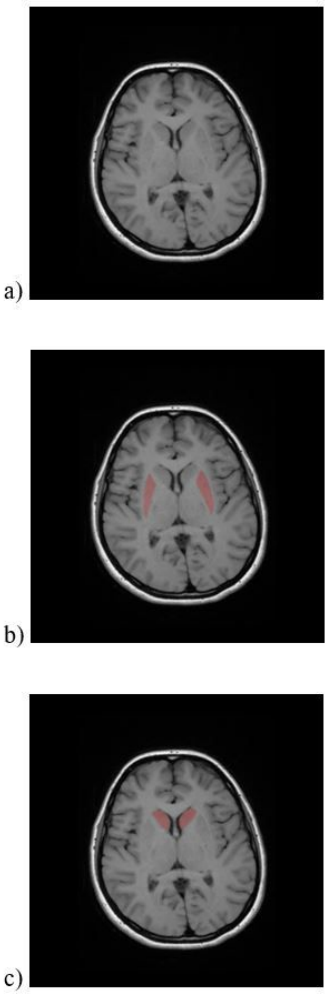

Figure 1

A cross-sectional brain image (a) selected for placement of ROIs in an individual and marked ROIs for putamen (b) and caudate (c) nuclei are shown.

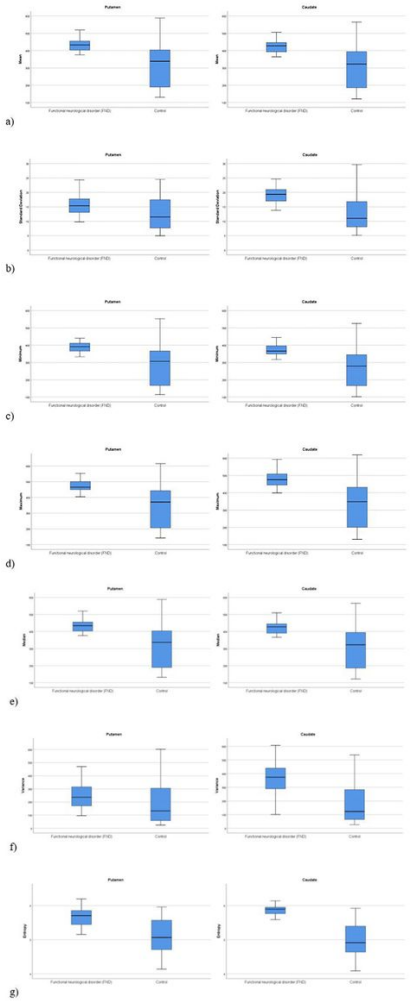

Figure 2

Distribution of mean (a), standard deviation (c), minimum (c), maximum (d), median (e), variance (f) and entropy (g) values of groups in putamen and caudate nuclei.

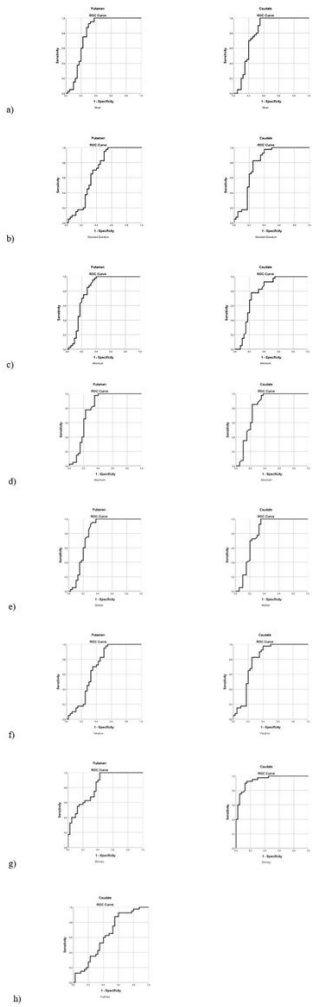

Figure 3

ROC analysis graphs that derived from putamen and caudate nuclei pixel values to distinguish study groups are shown: mean (a), standard deviation (c), minimum (c), maximum (d), median (e), variance (f), entropy (g) and kurtosis (h).